Hindawi
Advances in Civil Engineering
Volume 2019, Article ID 5818071, 9 pages
https://doi.org/10.1155/2019/5818071

Research Article

Cracking Mode Analysis of Crack Initiation in Rocks under Uniaxial Compression

Ye Lou, Guangqing Zhang, and Xiaoxiao Wang

College of Petroleum Engineering, China University of Petroleum, Beijing 102249, China

Correspondence should be addressed to Guangqing Zhang; zhangguangqing@cup.edu.cn

Received 31 August 2018; Revised 5 November 2018; Accepted 16 December 2018; Published 23 January 2019

Guest Editor: Guang Xu

Crack initiation is related to the behavior of the preexisting microcracks within a rock specimen, which suggests the specimen starts to fail. The determination of crack initiation stress is important for identifying the elastic stage and related mechanical parameters. Uniaxial compression tests with acoustic emission monitoring were performed to study crack initiation for tight sandstone, loose sandstone, and granite. The evolution of the cracking mode, i.e., the statistics of the cracking mode under compression, was obtained through modified acoustic emission parameter analysis. Based on the logarithm of the acoustic emission parameter (LAEP), a cracking mode analysis (CMA) method is proposed and used to determine the crack initiation stress. Results from the tests indicate that the crack initiation stress between the same rock specimens obtained by CMA is very close. The mean ratio of crack initiation stress to compression strength is 0.45, 0.34, and 0.35 for tight sandstone, loose sandstone, and granite, respectively. According to the results of CMA, crack volumetric strain (CVS) method, and lateral strain response (LSR) method, there is no big difference among those methods in tight sandstone and loose sandstone. In granite, the results obtained by CMA are close to those obtained by CVS, but smaller than those obtained by LSR. The CMA interprets the initiation of cracks from the fracture behavior of microcracks and is an objective method to determine the initiation stress.

1. Introduction

Unlike metals, rocks usually contain many microcracks. As early as the 1920s, Griffith proposed that such microcracks were capable of influencing the mechanical properties of rocks subjected to applied loads [1]. Under compression conditions, the failure process of the ultimate strength is currently divided into four stages: (1) crack closure stage, (2) elastic deformation stage, (3) crack stable growth stage, and (4) crack unstable growth stage [2, 3]. Many researchers have offered descriptions of the cracking modes during the process of rock failure [4, 5]. For rocks, the crack initiation stress is the first stress threshold for the stage division of the failure process and also plays a critical role in the determination of the mechanical parameters. Some studies have found that crack initiation in rock is closely related to spalling problems that occur during underground construction [6–8].

Since Brace first presented an approach to determine the crack initiation from volumetric strain in 1966, various crack initiation determination methods have been proposed [9]. For example, Lajtai and Stacey suggested different crack initiation point determination methods based on the radial strain [10, 11]; another crack initiation point determination method was proposed by Diederichs based on the variation in Poisson's ratio [12]. Martin identified the volumetric strain of cracks according to differences between volumetric strain and elastic strain and then determined the crack initiation through the changes in the volumetric strain of the cracks (CVS) [13]. However, these methods rely on the determination of both elasticity modulus and Poisson's ratio, and the parameters are affected by some subjective factors that induce errors [14]. At present, the lateral strain response (LSR) method proposed by Nicksiar and Martin can determine such point in a simple and effective manner [15]. The cumulative acoustic emission hit (CAEH) method has been developed for the determination of the crack initiation stress [16]. Additionally, the influences of subjective factors can be excluded by using those two approaches to objectively identify the crack initiation point [17].

Many researchers believe that rock failure is closely related to the mechanical behavior of microcracks, but there

has been a lack of effective observation methods. In the earliest studies of rock failure, the researchers used optical microscopes to observe microcrack morphology and structure [18]. With advancements of the technologies, computed tomography (CT) and scanning electron microscopy have been introduced to study the internal damage processes of rock specimens under stress [19, 20]. Nevertheless, applications of these techniques have some limitations. Continuous monitoring cannot be easily realized, and a considerable amount of time is required to conduct postprocessing and obtain the final test results. In contrast, acoustic emission (AE) testing provides advantages without affecting the loading process [21]. Acoustic emission is the transient elastic waves within a material, caused by the rapid release of localized stress energy [22]. Many researches have used AE techniques under uniaxial/triaxial conditions to study the failure of brittleness materials [23–25]. AE testing has also been applied to interpret the cracking modes of microcracks in laboratory tests [26–28]. A cracking mode study based on a signal-based analysis needs multiple sensors and takes much time for postprocessing [29]. Moreover, the analysis is often limited by the size of the rock specimens. A parametric AE analysis can be more convenient than signal-based analysis to identify cracking modes. Hence, a cracking mode analysis based on AE can be chosen to identify the crack initiation.

Although many methods for measuring crack initiation stress have been proposed and some models have been developed to interpret the crack initiation from volume change of microcracks, there is no accurate description of the fracture behavior of the microcracks. In this paper, the evolution of the cracking mode in the uniaxial compression test is studied by using AE parameters, and the crack initiation is interpreted from the fracture behavior of microcracks. An objective cracking determination method based on cracking mode analysis (CMA) is proposed, and its effectiveness is verified by comparing with the other method. This proves that it is reasonable to analyze the failure process of rock from the microcracks fracturing process. And it also provides a new angle for the determination of the other characteristic points of rock damage under compression.

2. Test Methods

2.1. Uniaxial Compression Tests. The test evaluated the specimens from three rock types: tight sandstone, loose sandstone, and granite. The basic properties of the rock specimens are presented in Table 1. While the tight sandstone specimens were acquired from coring at 3000 m underground, the loose sandstone and granite specimens were obtained from outcrops. Following the recommended standard of the International Society for Rock Mechanics (ISRM), the specimens were processed into cylindrical shapes with diameters of 25 mm and lengths twice the diameter, as presented in Table 1. The deviations between parallel top and bottom surfaces of any specimen were not allowed to exceed 2.5%.

During the uniaxial compression test, an AE acquisition instrument and two 7.8 mm diameter sensors were used to collect the AE waveform signals; the resonant frequency of the sensors is 150 kHz. The signal preamplifier of the AE monitoring system was 40 dB, and the corresponding signal sampling frequency was 5 MHz. After an ambient noise test, the measurement threshold value was set to 35 dB. The results of the three-point bending test show that, in the size range of the tested samples, the effect of the distortion on the AE parameters is not significant to the result of the cracking mode analysis (see Supplementary Test S1 in Supplementary File S1 online).

As shown in Figure 1, the radial and axial directions of the test were measured by linear variable differential transformers (LVDTs). A copper sleeve was bonded to a specimen surface that had been polished, and ultrasound couplant was then applied onto the surface of the AE sensor so that it could be mounted inside the copper sleeve. To diminish the disturbances from the friction generated between the specimen ends and compression plates on the test results, both ends of the specimen were lubricated with petrolatum. The uniaxial compression test was performed by a triaxial servo compression test system. The designed confining pressure was 200 MPa. The maximum axial load was 10000 kN, and the test ranges of the axial and radial deformations were from −2 mm to 2 mm. The signals such as the confining pressure, axial load, displacement, and strain were collected and controlled by the DOLI automatic data acquisition and control system. During the entire test process, displacement was employed to maintain the loading speed of 0.02 mm/s.

2.2. Cracking Mode Classification Based on Modified Parametric AE Analysis. During the process of rock failure, numerous microcracks are activated, consequently generating many AE signals due to the release of strain energy. The parameters of the AE signals vary with the cracking modes. Both average frequency (AF) and rise time over the maximum amplitude (RA) can be used as indexes to study the cracking mode through the differences between longitudinal and transverse wave velocities and the influence of different cracking modes on the frequency [30]. By referring to the recommended testing standard of concrete materials stipulated in the International Union of Laboratories and Experts in Construction Materials, Systems and Structures (RILEM), RA and AF can be defined as follows: RA is the rise time over the maximum amplitude and AF is the ratio of AE ringdown-counts over the duration of the signal [31]. The rise time (RT) is the duration from the onset time of the signals until the moment that the amplitude peaks. After the AE parameters have been treated with a moving average of per 0.1 second, they are distributed within an AF-RA coordinate plane. Subsequently, the cracking modes of the microcrack events can be determined according to the relative positions of the cracking mode classification lines (CMCLs) and AE parameters [32].

To study how the evolution of the cracking mode changes during rock loading, it is necessary to consider the variations in the AE parameters in the time domain. The AF-RA-time three-dimensional coordinate system based on the parametric AE analysis is too complex to be analyzed.

Table 1: Basic properties of the rock specimens.

Serial no. of specimen	Rock type	Porosity (%)	Grain size	Density (g/cm^3)	Image
A B C	Tight sandstone	7	Fine	2.57	
D E F G	Loose sandstone	12.3	Fine	2.18	
H I J	Granite	1.2	Fine to medium	2.78	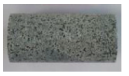

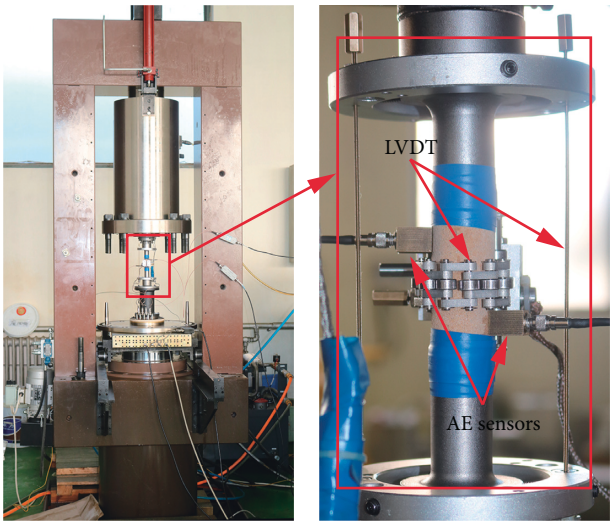

Figure 1: Uniaxial compression test setup.

Moreover, the existing method can only divide the cracking mode into two types, tensile-mixed and shear, and results for the same cracking mode are not easily compared. To solve this problem, we propose a parameter called the logarithm of the AE parameter (LAEP) (Equation (1)). For various microcracks with dissimilar cracking modes, the ratio of AF to RA may vary considerably. To better describe the trend of the differences in this ratio, the AF/RA ratio is processed logarithmically:

$$\mathrm{LAEP} = \log_{10}\left(\frac{\mathrm{AF}}{\mathrm{RA}}\right). \quad (1)$$

During uniaxial compression testing, crack initiation occurred and was followed by propagation and interconnection as the load increased. In addition, many AE signals were generated during this process. The characteristics of these AE signals changed due to the differences in the focal mechanisms. Although the CMCL value for each specimen is not easy to determine, a decrease in the LAEP suggests that the cracking mode has a shear failure trend, while an increase in the LAEP suggests that the cracking mode has a tensile or mixed mode trend. In addition, it can be inferred that not only the CMCL values may vary, but the upper and lower limits of the corresponding LAEP values may also change due to the differences in the compositions and microstructures of the rock types.

Combine with Ohno's research [33], the distribution of the LAEP values is divided into two parts that correspond to different fracture behaviors, as shown in Figure 2. When stress is applied normally to the microcrack, the microcrack cannot be activated, and there is no AE signal. With a change in the stress, compression-shear failure occurs along the microcracks, and the LAEP increases gradually from a minimum value. When the LAEP is above the CMCL, the tensile-shear failure will occur. In addition, the maximum value of the LAEP is obtained when pure mode I fracturing occurs.

The cracking mode analysis based on LAEP can be used to not only distinguish fracture behaviors but also perform an analytical investigation on the mechanical responses of rocks during the whole loading process.

3. Proposed Cracking Mode Analysis (CMA) Method and Verification

3.1. Cracking Mode of Microcracks under Compression. Due to the influences of various diagenetic conditions, there exist many pores and microcracks in rocks. Considering that the tensile strength of a rock material is generally far less than its compressive strength, tensile failure will preferentially occur in the pore structure under compression. Compared with this pore structure failure, microcracks are considerably more complicated. Hence, the mechanical behavior of a single crack under triaxial compression needs to be studied.

The microcracks will be closed first when rock is under compression. As shown in Figure 3, the stress state along a closed fracture plane will be discussed below by taking a two-principal-stress state microelement in the sample.

Under the action of stresses perpendicular to the fracture plane, the stress of the friction generated on this plane can be denoted as

$$\tau_n = \begin{cases} 0, & k \le -\tan^2\beta, \\ f\sigma_n = \dfrac{1}{2}\sigma f\left[(1+k) - (1-k)\cos 2\beta\right], & k \le -\tan^2\beta. \end{cases} \quad (2)$$

The effective shear stress of this plane is $\tau_{\mathrm{ef}} = \tau_{xy} - \tau_n$.

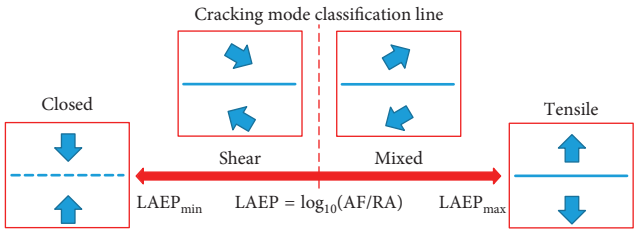

Figure 2: The definition of the parameter LAEP.

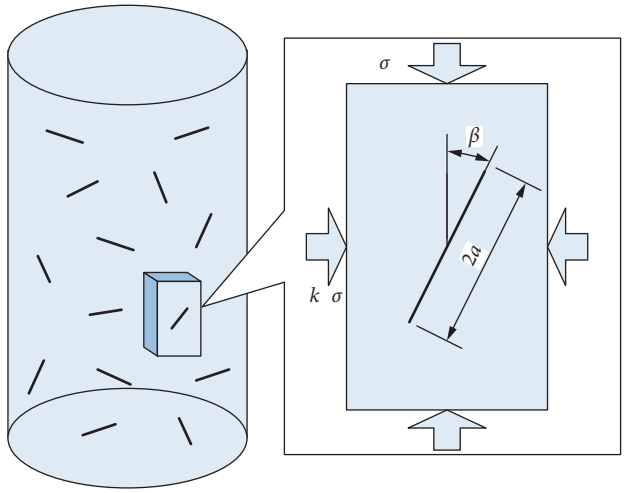

Figure 3: Internal stress state of the rocks near the microcrack.

$$\tau_{ef} = \begin{cases} \frac{1}{2}\sigma(1-k)\sin 2\beta, & k \le -\tan^2\beta, \\ \frac{1}{2}\sigma\{(1-k)\sin 2\beta & \\ \quad - f[(1+k)-(1-k)\cos 2\beta]\}, & k \le -\tan^2\beta. \end{cases} \tag{3}$$

For a closed fracture plane under compression, only mode II fracturing is assumed, and the stress intensity factor at the crack tips is expressed as $K_{II} = \tau_{ef}\sqrt{\pi a}$. When $K_{II} = K_{IIC}$, the crack begins to propagate; the following equation can be established for the critical condition:

$$\sigma_c = \frac{2K_{IIC}}{\sqrt{\pi a}} \cdot \frac{1}{(1-k)\sin 2\beta - f[(1+k)-(1-k)\cos 2\beta]}. \tag{4}$$

The function must satisfy the condition of $0 < k < 2f^2 + 1 - 2f\sqrt{f^2+1}$.

σ_c is the critical shear stress of the crack, and f is the coefficient of friction. K_{IIC} is the mode II fracture toughness and is usually a material constant.

At the microscopic scale, the differences in the microcrack lengths are small enough and can be approximated as a constant value. Here, the stress of the friction on the crack surface is assumed to be uniform; then, f is only associated with the material and is also a constant. So through equation (4), we can get the curves between critical shear stress and crack dip at different stress ratios as shown in Figure 4, and

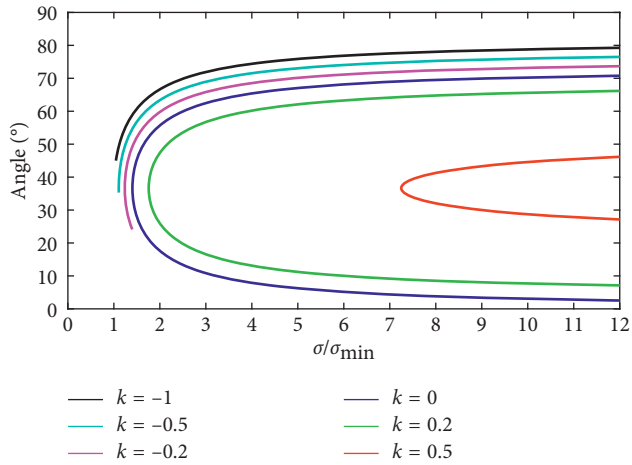

Figure 4: Relation between critical shear stress and crack dip at different stress ratios.

σ_c is normalized. Figure 4 reveals that as k increases from negative to positive, the minimum value of σ_c, which is the critical shear stress of the microcrack, also increases. When k is negative and the microelement is under a lateral tensile stress, the stress-fracture dip curves are asymmetrical; however, if k is positive, which indicates that the microelement is under a lateral compressed stress, these curves are symmetric. With a continued increase in stress, shearing occurs along the microcracks at successive angles. The curves in Figure 4 clearly show two limit values of the microcrack fracture dip, β_{min} and β_{max}, signifying that, theoretically, no mode II fracturing occurs along microcracks with dips outside of this range, no matter the stress magnitude. During the loading of a uniaxial compression test, the initiation of many microcracks with dip angles between β_{min} and β_{max} occurs as the stress σ increases. When shear failure occurs along nearly all the microcracks within the range $[\beta_{min}, \beta_{max}]$ and σ reaches a certain value, crack initiation begins.

Additionally, Figure 4 indicates that when $k > 0$, the critical stress is infinite and the dip angle approaches β_{min}. In this case, mode II fractures are less likely to be activated. However, the cracks usually show strong instability, and tensile fractures may also form because of the decrease in the fracture dip β. The probable causes of such a phenomenon are described as follows. When β is sufficiently low, the microcracks cannot be considered closed. And there is no friction between the fracture planes; in this case, microcrack opening often increases with additional tensile stress, which can cause mode I fracturing.

The critical stress will reach a minimum when the microcracks are at a certain angle. At this moment, $\partial\sigma/\partial\beta = 0$ and $\partial^2\sigma/\partial^2\beta > 0$. Therefore, an expression for the initial crack angle can be acquired:

$$\beta_{\sigma-min} = \frac{1}{2} \cdot \arctan\frac{1}{f}. \tag{5}$$

As shown in Figure 5, the initial angle $\beta_{\sigma-min}$ monotonically changes with f, which is the friction coefficient of the fracture plane and is independent of the stress ratio k.

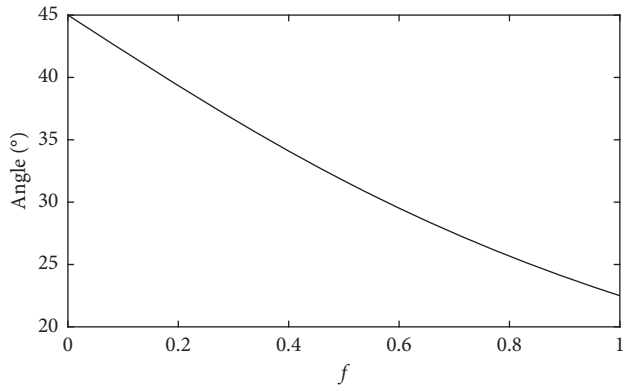

Figure 5: Relationship between friction coefficient and initial angle of crack formation.

Therefore, variations in f affect $\beta_{\sigma-\min}$ without changing the functional relationship between σ and initial angle. The dip range $[\beta_{\min}, \beta_{\max}]$ of cracks in specimens from the same rock should be the same, and the crack initiation stress should be well determined, provided that the crack initiation stress is related to only the material.

3.2. Crack Initiation Determination by CMA Method. As mentioned above, shear failure of microcrack under compressive stress occurs sequentially with a certain range of microcrack dip angles. Such a process is not completed until all those microcracks have been activated. In this case, the microcracks inside the rock can be considered fully initiated, corresponding to crack initiation. Therefore, it may be feasible to distinguish different rock failure stages by analyzing the cracking modes of microcracks during compressing. The cracking mode analysis is based on the analysis of LAEP. As the uniaxial compression increases, shearing successively occurs along the closed microcracks within a range of dip angles because of differences in the stress states of the fracture planes; the corresponding LAEP thus gradually decreases. After the LAEP and the corresponding cracking mode were analyzed, the variations in the LAEP during loading were utilized to study the internal microcrack responses of the rocks and the impacts of these responses on the mechanical behaviors of the specimens.

Figure 6 shows the time-varying LAEP distribution and variations in stress for the three rock types. The figure provides three representative test results, while the results of all ten rock specimens can be found in Supplementary Figures S2 to S4 in Supplementary File S1. Figure 6(a) shows that the LAEP values of the tight sandstone vary from 0 to 4. During the early stage of loading, the LAEP distribution is relatively concentrated; it fell slightly within a short time period, which was followed by an upward trend. This indicates that, in this stage, the microcracks are gradually closed, and the cracking mode changes from tensile to shear. With the increase in loading, the distribution of LAEP is more disperse, and the lower envelope of LAEP appears to decrease first and then increase. Generally, the macrocracks of the rock are assumed to form when the ultimate strength is reached; then, the friction between fracture planes begins to play a dominant role. Hence, the AE signals are mainly generated by shear slip after the stress has reached the ultimate strength. That is the main reason the distribution of the LAEP value is more concentrated and obviously decreases after the ultimate strength when the stress is close to the ultimate strength. In Figure 6(b), the distribution of the LAEP for the loose sandstone is more disperse and greater than that of the tight sandstone, ranging from 0 to 6. Due to the existence of a large number of pores in the loose sandstone, tensile failure caused by pore failure occurs during loading. Despite the strength limit, LAEP still has a higher value. Although the load is close to the ultimate strength, there still exists a large value of LAEP. Similar to those tight sandstones, the lower envelope of LAEP also appears to decrease first and then increase. Figure 6(c) shows that the distribution of LAEP in granite samples is more concentrated, ranging from 1.5 to 3.5. Overall, the variation characteristics are similar to those of loose sandstone, but the minimum of the lower envelope appears earlier.

Whatever the rock type is, a comparison of the diagrams in Figures 6(a)–6(c) shows that the variations in the LAEP envelope tend to first decrease and then increase. Additionally, the minimum envelope value is sometimes recorded during the early stage of loading. Considering that such cases always happen when the rock is in an unstable loading stage, these minima may be caused by friction at the sample faces. Without regarding the minimum envelope values at the beginning, the lowest point of the envelope during the loading process also signifies that microcracks shearing has nearly finished in the rock. The stress that corresponds to the lowest point of the LAEP envelope is the crack initiation stress. After crack initiation, the tensile cracks parallel to the direction of the maximum stress form at or near both ends of the microcracks. The propagation of these tensile cracks corresponds to a stable propagation stage.

According to the above analysis, the changes in the LAEP are consistent with the mode of the microcrack failure within the rock. The LAEP is correlated with the stress state of the microcracks because the lowest point of the LAEP envelope corresponds to the sufficient occurrence of microcrack shear failure within the rock. The effective shear stress on a microcrack plane during mode II fracturing is defined as $\tau_c = K_{IIC}/\sqrt{\pi a}$, where K_{IIC} refers to the roughness constant of the mode II fracture. Furthermore, assuming that the crack length is finite, τ_c is also a specified value at the time of crack shearing. Therefore, no matter how σ changes, the shear strength of the crack τ_c remains unchanged and, thus, does not impact the changes in the LAEP during the test.

As previously described, as σ increases, the microcracks under compression successively shear according to the dip angles. For microcracks of an identical length, mode II fracturing occurs when τ_{ef} reaches τ_c on the fracture plane. The effective stress along the fracture plane can be expressed as $\tau_{ef} = \tau_{xy} - \tau_n$. Although the shear strengths of the cracks are identical when mode II fracturing occurs, equations (2) and (3) indicate that τ_{xy} and τ_n will vary with the crack dip angles and applied stress. Furthermore, considering $\tau_n = \tau_{xy} - \tau_c = f\sigma_n$, the LAEP is inferred to be associated with τ_n: LAEP $\propto 1/\tau_n$. In other words, the LAEP may be

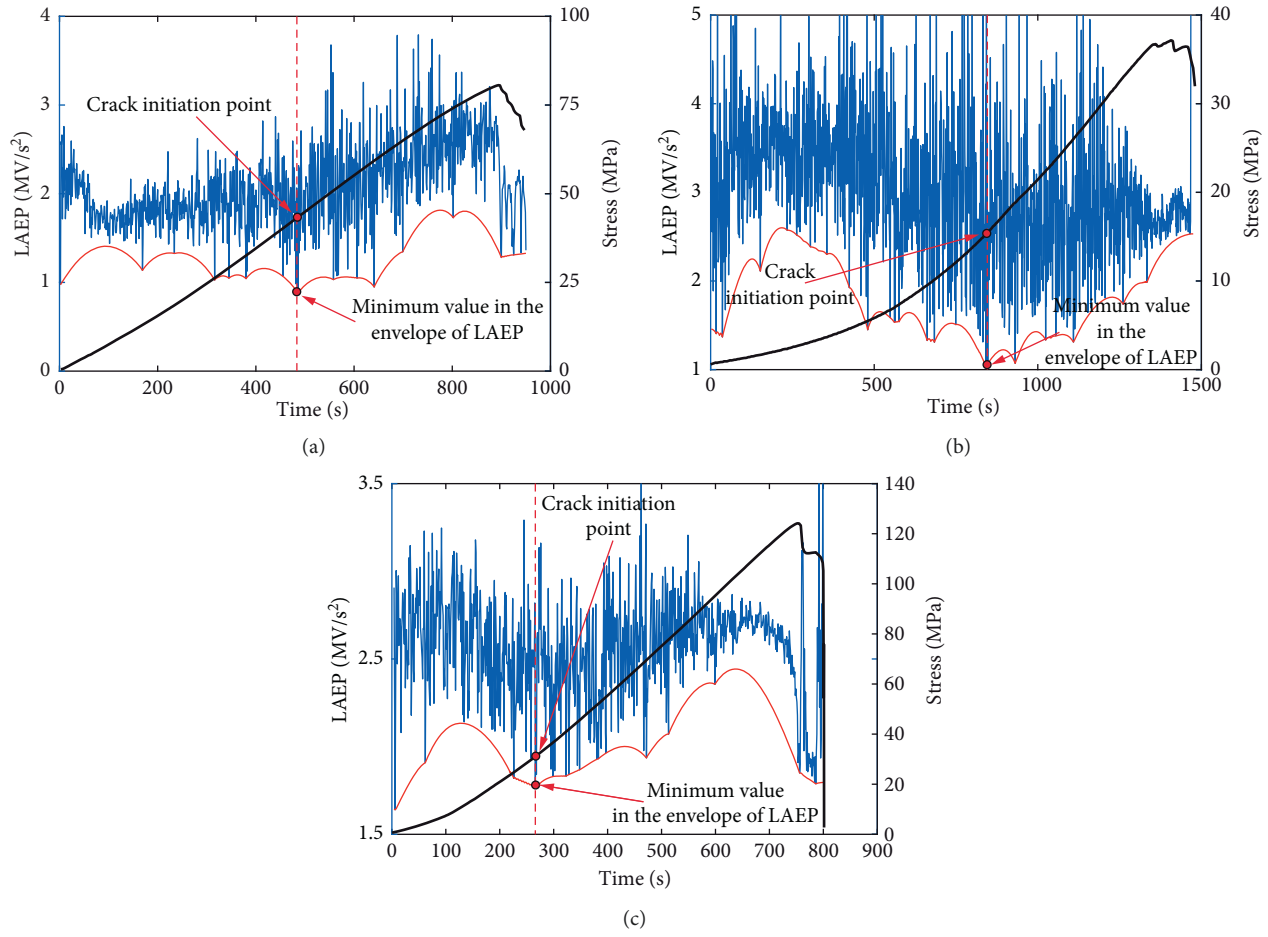

Figure 6: Time-varying LAEP, lower envelope, and stress distribution of the specimens under compression. (a) Tight sandstone. (b) Loose sandstone. (c) Granite.

affected by the force of friction along the cracks and the stress applied normal to the fracture plane. To determine the specific functional relationships, these parameters need to be further theoretically and experimentally studied.

3.3. Comparison and Verification. The mechanical parameters and crack initiation stress measured under uniaxial compression for the three rock types are listed in Table 2. "CMA" in the table represents that the crack initiation stresses are calculated using the CMA method described above. The crack initiation stresses, determined by the CVS method proposed by Martin [13] in 1993 and the LSR [15] method, are also presented in Table 2. Figure 7 shows those different methods for determining crack initiation stress of rocks under uniaxial compression. The "Stress ratio" in the table denotes the ratio of the crack initiation stress to the compression strength. The mean value of the stress ratio is the ratio of the mean crack initiation stress to the mean compression strength.

In Table 2, due to the difference in the coring depth, the mechanical parameters of tight sandstones vary in both elastic modulus and ultimate strength. However, significant differences in the elastic modulus among the three types of rock can be observed. The loose sandstone has the highest degree of porosity, and its mean elastic modulus is the lowest, 5.4 GPa. The granite has the highest mean elastic modulus, 40.4 GPa. The compressive strength is consistent with the elastic modulus. The highest is granite, 116.4 MPa, followed by tight sandstone, 85.6 MPa. The lowest is loose sandstone, 32.5 MPa. In addition, the strength of the loose sandstone specimens shows some difference between specimens D and E and specimens F and G. Such differences may be caused by variations in the coring direction. Specimens D and E were cored perpendicular to the sedimentation direction, while specimens F and G were cored parallel to the sedimentation direction.

As shown in Figure 8, comparing the initiation stress of different rock types calculated by using the CMA method, it has great difference, but the minor differences between stress ratios of different rock types. Those ratios are 0.34, 0.45, and 0.35 for tight sandstone, loose sandstone, and granite, respectively. And then, we compare the results obtained by different methods. For tight sandstones, there is little difference in the mean value of the crack initiation stress calculated by different methods, which is maintained at approximately 40% of the ultimate strength. For loose sandstone, the mean value of the crack initiation stress

Table 2: Comparisons of the results used for determining the crack initiation stress.

No.	Rock type	E (GPa)	μ	Strength (MPa)	CMA		CVS		LSR	
					Stress (MPa)	Stress ratio	Stress (MPa)	Stress ratio	Stress (MPa)	Stress ratio
A	Tight sandstone	18.3	0.17	80.6	43.3	0.54	30.8	0.38	31.1	0.39
B		23.4	0.16	103.8	32.6	0.31	37.7	0.36	37.1	0.36
C		14.3	0.13	72.2	36.2	0.50	29.8	0.41	33.2	0.46
Mean		18.7	0.16	85.6	37.4	0.45	32.8	0.39	33.8	0.40
D	Loose sandstone	5.2	0.40	27.3	9.3	0.34	10.9	0.40	9.2	0.34
E		4.9	0.28	29.5	6.4	0.22	10.5	0.35	9.9	0.34
F		5.5	0.35	36.8	15.2	0.41	14.0	0.38	8.6	0.23
G		5.9	0.42	36.4	14.0	0.39	13.6	0.37	12.3	0.34
Mean		5.4	0.36	32.5	11.3	0.34	13.1	0.40	10.0	0.31
H	Granite	41.9	0.21	123.0	40.13	0.33	49.4	0.40	58.5	0.48
I		41.4	0.19	124.1	31.21	0.32	40.3	0.32	62.9	0.51
J	Granite	38.0	0.17	102.0	40.52	0.40	41.1	0.40	66.4	0.65
Mean		40.4	0.19	116.4	37.29	0.35	43.6	0.38	62.6	0.54

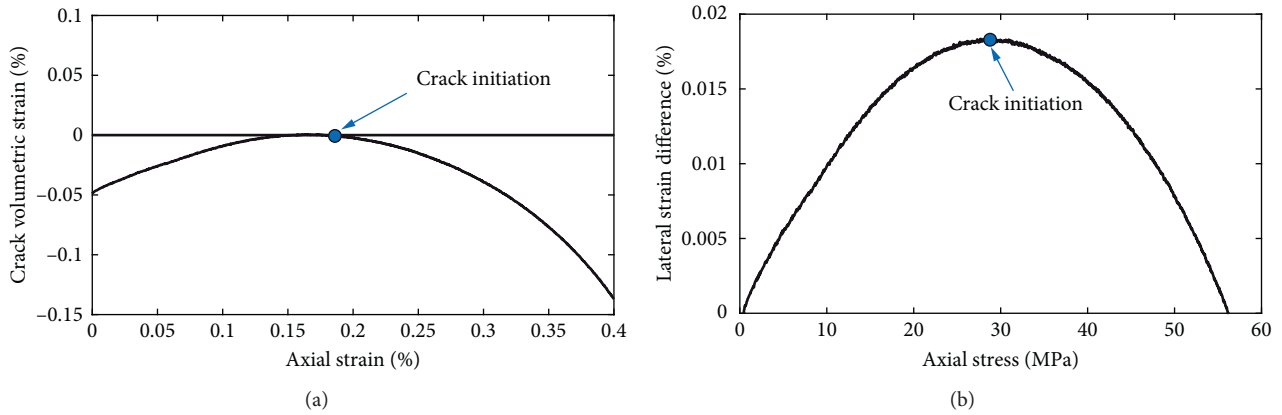

Figure 7: Crack initiation stress determination from uniaxial testing conducted with different methods. (a) CVS method [13]. (b) LSR method [15].

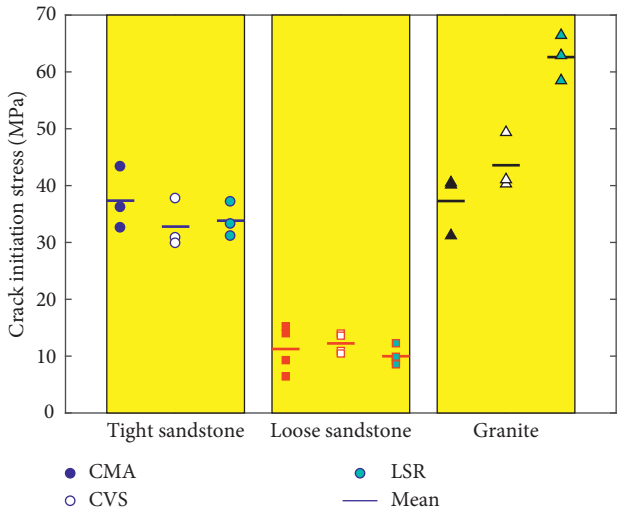

Figure 8: Comparison of crack initiation stresses obtained from different rock specimens and methods.

calculated by the CVS method is slightly higher, but it is not more than 40% of the ultimate strength. For granite, the result of the LSR method is obviously higher than that of the other two methods, reaching approximately 50% of the strength limit.

A more intuitive comparison among the results obtained from these three methods is shown in Figure 8. The results of all three methods are similar for the crack initiation stresses of the tight and loose sandstones. As mentioned before, for granite, the results of the LSR method are clearly different from the results achieved by using the CMA method and CVS method. Such a difference may exist because the mineral constituents and internal structures of the rock types are distinct, which requires further study and determination. The abovementioned results verify not only the validity of the microcrack model but also the feasibility of using the LAEP to determine the crack initiation points.

4. Conclusions

Failure of rocks under compression is of great importance for building and underground construction. However, the initiation and subsequent propagation of the cracks are important to the damage and failure of a material. In this paper, the cracking mode of microcracks initiation within rocks under uniaxial compression is studied theoretically and experimentally.

Theoretical analyzes show that not all the closed microcracks will be activated by shear during the compressing process of rock specimens. Shear slip of the microcracks occurs in sequence when the microcracks dip varies in a certain range. If these microcracks are completely activated by shear, the crack initiation begins. At this point, the critical stress of shear failure reaches the maximum. After that, the microcracks begin a stable tensile propagation stage.

A modified parametric AE analysis method was proposed in this paper to analyze the cracking mode evolution of microcracks during the uniaxial compression tests. The key of this method is to propose a new parameter LAEP that is sensitive to the fracture mode. The test results reveal that successive crack shearing is accompanied by a gradual decrease of LAEP, which ultimately reaches a minimum. In conjunction with the theoretical analysis, the minimum value in the envelope of LAEP in fact corresponds to the crack initiation point.

Although the compressive strength and crack initiation stress of three rock types are quite different, the ratio of crack initiation stress to compressive strength is very close. Those ratios are 0.34, 0.45, and 0.35 for tight sandstone, loose sandstone, and granite, respectively. By comparing the results of the CMA method with CVS and LSR methods, the validity of this method is verified. This study demonstrates the feasibility of interpreting crack initiation from a microperspective, and a new CMA method has been developed for objective determination of the crack initiation stress.

Data Availability

All data are included in the manuscript as tables and figures. All results for the cracking mode analysis are separately included in the electronic supplementary material.

Conflicts of Interest

The authors declare that there are no conflicts of interest regarding the publication of this paper.

Acknowledgments

We thank Dr. Lili Tan for very instructive discussions.

Supplementary Materials

Additional information on the effect of wave distortion on AE characterization is provided. And the LAEP (logarithm of the AE parameter) and envelope line of each rock sample are presented. (*Supplementary Materials*)

References

[1] A. A. Griffith, "The phenomena of rupture and flow in solids," *Philosophical Transactions of the Royal Society of London. Series A, Containing Papers of a Mathematical or Physical Cxharacter*, vol. 221, no. 582–593, pp. 163–198, 1921.

[2] Z. T. Bieniawski, "Mechanism of brittle fracture of rock: part II—experimental studies," *International Journal of Rock Mechanics and Mining Sciences & Geomechanics Abstracts*, vol. 4, no. 4, pp. 407–423, 1967.

[3] M. Cai, P. K. Kaiser, Y. Tasaka et al., "Generalized crack initiation and crack damage stress thresholds of brittle rock masses near underground excavations," *International Journal of Rock Mechanics and Mining Sciences*, vol. 41, no. 5, pp. 833–847, 2004.

[4] J. Akbardoost and M. R. Ayatollahi, "Experimental analysis of mixed mode crack propagation in brittle rocks: the effect of non-singular terms," *Engineering Fracture Mechanics*, vol. 129, pp. 77–89, 2014.

[5] F. Dai, M. D. Wei, N. W. Xu et al., "Numerical assessment of the progressive rock fracture mechanism of cracked chevron notched Brazilian disc specimens," *Rock Mechanics and Rock Engineering*, vol. 48, no. 2, pp. 463–479, 2015.

[6] C. D. Martin, "Seventeenth Canadian geotechnical colloquium: the effect of cohesion loss and stress path on brittle rock strength," *Canadian Geotechnical Journal*, vol. 34, no. 5, pp. 698–725, 1997.

[7] M. S. Diederichs, "The 2003 Canadian geotechnical colloquium: mechanistic interpretation and practical application of damage and spalling prediction criteria for deep tunnelling," *Canadian Geotechnical Journal*, vol. 44, no. 9, pp. 1082–1116, 2007.

[8] C. D. Martin and R. Christiansson, "Estimating the potential for spalling around a deep nuclear waste repository in crystalline rock," *International Journal of Rock Mechanics & Mining Sciences*, vol. 46, no. 2, pp. 219–228, 2009.

[9] W. Brace, B. Paulding, and C. Scholz, "Dilatancy in the fracture of crystalline rocks," *Journal of Geophysical Research*, vol. 71, no. 16, pp. 3939–3953, 1966.

[10] E. Lajtai, "Brittle fracture in compression," *International Journal of Fracture*, vol. 10, no. 4, pp. 525–536, 1974.

[11] T. Stacey, "A simple extension strain criterion for fracture of brittle rock," *International Journal of Rock Mechanics and Mining Sciences & Geomechanics Abstracts*, vol. 18, no. 6, pp. 469–474, 1981.

[12] M. Diederichs, P. Kaiser, and E. Eberhardt, "Damage initiation and propagation in hard rock during tunnelling and the influence of near-face stress rotation," *International Journal of Rock Mechanics and Mining Sciences*, vol. 41, no. 5, pp. 785–812, 2004.

[13] C. Martin and N. Chandler, "The progressive fracture of Lac du Bonnet granite," *International Journal of Rock Mechanics and Mining Sciences & Geomechanics Abstracts*, vol. 31, no. 6, pp. 643–659, 1994.

[14] E. Eberhardt, D. Stead, B. Stimpson, and R. S. Read, "Identifying crack initiation and propagation thresholds in brittle rock," *Canadian Geotechnical Journal*, vol. 35, no. 2, pp. 222–233, 1998.

[15] M. Nicksiar and C. Martin, "Evaluation of methods for determining crack initiation in compression tests on low-porosity rocks," *Rock Mechanics and Rock Engineering*, vol. 45, no. 4, pp. 607–617, 2012.

[16] X. G. Zhao, M. Cai, J. Wang et al., "Objective determination of crack initiation stress of brittle rocks under compression using AE measurement," *Rock Mechanics and Rock Engineering*, vol. 48, no. 6, pp. 2473–2484, 2015.

[17] W. Tao, H. Tang, J. Ma et al., "Evaluation of methods for determining crack initiation stress under compression," *Engineering Geology*, vol. 235, pp. 81–97, 2018.

[18] J. F. Labuz, S. P. Shah, and C. H. Dowding, "Experimental analysis of crack propagation in granite," *International*

Journal of Rock Mechanics and Mining Sciences & Geomechanics Abstracts, vol. 22, no. 2, pp. 85–98, 1985.

[19] S. Q. Yang, "Fracturing mechanism of compressed hollow-cylinder sandstone evaluated by X-ray micro-CT scanning," *Rock Mechanics and Rock Engineering*, vol. 51, no. 7, pp. 2033–2053, 2018.

[20] Z. Yu, P. J. Jin, X. U. Wei-Ya et al., "Experimental study of triaxial creep behavior and long-term strength of clastic rock in dam foundation," *Rock and Soil Mechanics*, vol. 37, no. 5, pp. 1291–1300, 2016.

[21] M. Ohtsu, *Acoustic Emission and Related Non-Destructive Evaluation Techniques in the Fracture Mechanics of Concrete: Fundamentals and Applications*, Woodhead Publishing, Sawston, UK, 2015, https://www.elsevier.com/books/acoustic-emission-and-related-non-destructive-evaluation-techniques-in-the-fracture-mechanics-of-concrete/ohtsu/978-1-78242-345-4.

[22] D. Lockner, "The role of acoustic emission in the study of rock fracture," *International Journal of Rock Mechanics and Mining Sciences & Geomechanics Abstracts*, vol. 30, no. 7, pp. 883–899, 1993.

[23] D. A. Lockner, J. D. Byerlee, V. Kuksenko, A. Ponomarev, and A. Sidorin, "Quasi-static fault growth and shear fracture energy in granite," *Nature*, vol. 350, no. 6313, pp. 39–42, 1991.

[24] K. Mogi, *Experimental Rock Mechanics*, CRC Press, Boca Raton, FL, USA, 2007, https://www.crcpress.com/Experimental-Rock-Mechanics/Mogi/p/book/9780415394437.

[25] O. V. Recently, "Nondestructive investigation of stress-induced damage in concrete," *Advances in Civil Engineering*, vol. 2010, Article ID 740189, 9 pages, 2010.

[26] M. Ohtsu, "Simplified moment tensor analysis and unified decomposition of acoustic emission source: application to in situ hydrofracturing test," *Journal of Geophysical Research: Solid Earth*, vol. 96, no. 4, pp. 6211–6221, 1991.

[27] M. Ohtsu, T. Okamoto, and S. Yuyama, "Moment tensor analysis of acoustic emission for cracking mechanisms in concrete," *ACI Structural Journal*, vol. 95, no. 2, pp. 87–95, 1998.

[28] T. Ishida, J. F. Labuz, G. Manthei et al., "ISRM suggested method for laboratory acoustic emission monitoring," *Rock Mechanics and Rock Engineering*, vol. 50, no. 3, pp. 665–674, 2017.

[29] C. U. Grosse and M. Ohtsu, *Acoustic Emission Testing*, Springer Science & Business Media, Berlin, Germany, 2008, https://link.springer.com/book/10.1007/978-3-540-69972-9.

[30] D. G. Aggelis, "Classification of cracking mode in concrete by acoustic emission parameters," *Mechanics Research Communications*, vol. 38, no. 3, pp. 153–157, 2011.

[31] M. Ohtsu, "Recommendation of RILEM TC 212-ACD: acoustic emission and related NDE techniques for crack detection and damage evaluation in concrete," *Materials and Structures*, vol. 43, no. 9, pp. 1187–1189, 2010.

[32] D. Aggelis, A. Mpalaskas, D. Ntalakas, and T. Matikas, "Effect of wave distortion on acoustic emission characterization of cementitious materials," *Construction and Building Materials*, vol. 35, pp. 183–190, 2012.

[33] K. Ohno and M. Ohtsu, "Crack classification in concrete based on acoustic emission," *Construction and Building Materials*, vol. 24, no. 12, pp. 2339–2346, 2010.